NANO-MICRO LETTERS

Vol. 2, No. 4
296-305 (2010)

Fabrication of a Highly Sensitive Hydrazine Electrochemical Sensor Based on Bimetallic Au-Pt Hybrid Nanocomposite onto Modified Electrode

Azadeh Azadbakht[1,*] and Amir Reza Abbasi[2]

In this research a novel nickel complex was used as electrocatalyst for electrooxidation of hydrazine. A nano-structured nickel-complex was electrodeposited on a bimetallic Au-Pt inorganic-organic hybrid nanocomposite modified electrode. The electrode possesses a three-dimensional (3D) porous network nanoarchitecture, in which the bimetallic Au-Pt NPs serving as metal nanoparticle based microelectrode ensembles are distributed in the matrix of interlaced 3, 3′, 5, 5′-Tetramethylbenzidine (TMB) organic nanofibers (NFs). Surface structure and composition of the sensor was characterized by scanning electron microscopy. Electrocatalytic oxidation of hydrazine on the surface of modified electrode was investigated with cyclic voltammetry method. The results showed that the nickel-complex films displayed excellent electrochemical catalytic activities towards hydrazine oxidation. The hydrodynamic amperometry at rotating modified electrode at constant potential versus reference electrode was used for detection of hydrazine. Under optimized conditions the calibration plots were linear in the concentration range of 0.2-85 µM and detection limit was found to be 0.1 µM. The modified electrode exhibited reproducible behavior and a high level stability during the electrochemical experiments, making it particularly suitable for the analytical purposes.

Keywords: 3, 3′, 5, 5′-Tetramethylbenzidine; Hydrazine; Nanocomposite electrodes; Nanofiber

Citation: Azadeh Azadbakht and Amir Reza Abbasi, "Fabrication of a highly Sensitive hydrazine electrochemical sensor based on bimetallic Au-Pt hybrid nanocomposite onto modified electrode", Nano-Micro Lett. 2, 296-305 (2010). doi:10.3786/nml.v2i4.p296-305

Hydrazine is a highly reactive molecule that can be used in agriculture as pesticides, blowing agents, pharmaceutical intermediates, photographic chemical, water treatment for corrosion protection and textile dyes [1]. Hydrazine is also an ideal fuel for a direct fuel cell system because its fuel electrooxidation process does not bring about any poisoning effects [1, 2]. There are several reported techniques for the determination of hydrazine, such as titrimetry [3], potentiometry [4], fluorimetry [1], spectrophotometry [5] and chemi-luminescence [6]. Voltammetric method possesses many advantages such as high sensitivity, good selectivity, rapid response and simple operating procedure. Because of the large overpotential of hydrazine oxidation at conventional electrodes, various inorganic and organic materials have been modified on the electrode surface to enhance the electron transfer rate and to reduce the overpotential for the oxidation of hydrazine [7-9]. In the electrochemical oxidation of hydrazine, the electrode material is clearly an important parameter where a high efficient electrocatalyst is needed. Hence, finding new electrode material for hydrazine determination is still of great interest. Nickel macrocyclic complexes can be easily electrodeposited onto an electrode surface in alkaline solution to form modified electrodes. This kind of modified electrode shows high catalytic activity toward electro-oxidation of organics containing OH and NH_2

[1]Department of Chemistry, Faculty of Basic Science, Islamic Azad University, Khorramabad Branch, Khorramabad, Islamic Republic of Iran
[2]Faculty of Science and Engineering, Islamic Azad University, Doroud Branch, Doroud, Islamic Republic of Iran
*Corresponding author. E-mail: Azadeh_Azadbakht@yahoo.com

groups, such as methanol, carbohydrates and amino acids [10, 11].

Over the past decade, one-dimensional (1D) inorganic-organic hybrid nanomaterials have received much interest because of their intriguing properties and potential applications in chemical or biochemical sensors, catalysis and nanodevices [12-19]. These hybrid materials based on the combination of organic and inorganic species exhibit the advantages over organic materials such as light weight, flexibility and good moldability, and inorganic materials such as high strength, heat stability and chemical resistance [20-22]. Such features of (1D) organic-inorganic hybrid nanomaterials make them ideal building blocks for a new generation of electrochemical sensors. Recently, Gong, and his co-workers developed a hybrid of bimetallic-inorganic-organic nanofibers (NFs) for the stripping assay of Hg (II) [23]. Decoration of organic nanowires with metal NPs could be an attractive route to fabricate inorganic-organic hybrid nanomaterials without compromising the functions of the nanowires or nanoparticles [14]. Nanoparticles frequently display unusual physical and chemical properties depending upon their size, shape and stabilizing agents. Nanoparticles also facilitate the electron transfer and can be easily modified with a wide range of biomolecules and chemical ligands. Electrochemical behavior and applications of nanoparticles have witnessed a significant growth in the past few years. Therefore combination of nanowires and metal nanoparticle have received much interest because of their intriguing properties and potential applications in chemical sensing [24, 25]. A 3,3,5,5-Tetramethylbenzidine (TMB), much less hazardous than benzidine and more sensitive as a chromogenic reagent, has been investigated for many years [26]. Doping of TMB-based organic nanofibers (NFs) with in-corporating of metals ions is of particular interest. In this paper, we report the electrodeposition of Nickel-2, 6-Diaminopyridine (Ni-DAP) on bimetallic Au-Pt inorganic-organic hybrid nano-composite glassy carbon electrode in alkaline solutions to form stable modified electrodes in order to catalyze the oxidation of hydrazine. Due to the excellent properties of selected hybrid nanocomposite the sensor exhibits a remarkable and stable current response.

Experiments

Chemicals and reagents

TMB and H_2PtCl_6 were purchased from Merck. $HAuCl_4$ was obtained from Aldrich. Hydrazine was obtained from Sigma. KOH, NaOH, KCl and other reagents were analytical grade from Merck. All other chemicals were of analytical-reagent grade and used without further purification.

Instrumentation

Electrochemical experiments were performed via using an Autolab modular electrochemical system (Eco Chem. Utrecht, The Netherlands) equipped with PSTA 20 model and driven by GPES software (Eco Chem.). A conventional three-electrode cell was used with a saturated Ag|AgCl as reference electrode, a Pt wire as counter electrode and a modified glassy carbon electrode as working electrode. All experiments were carried out at ambient temperature of 20 ± 1°C. A Metrohm pH-meter (model 691) was also applied for the pH measurements. The surface morphology of modified electrodes was characterized with a scanning electron microscope (SEM, Philips XL 30) with gold coating.

Synthesis of gold nanoparticle

In this study, colloidal gold nanoparticles were prepared in accordance with the literature published before [27]. 0.5 ml of 1% (w/v) of sodium citrate solution was added to 50 ml of 0.01% (w/v) of $HAuCl_4$ boiling solution. $HAuCl_4$ and sodium citrate aqueous solutions were filtered through a 0.22 μm microporous membrane filter before use. In this procedure, all glass wares used were cleaned in freshly prepared 1:3 of HNO_3/HCl solution and then rinsed thoroughly with doubly distilled water. The mixture was boiled for 15 min and then stirred for 15 min after removing the heating source to produce colloidal gold nanoparticles. The solution was stored in a refrigerator in a dark-colored glass bottle before use. The synthesized colloidal gold nanoparticles show maximum absorbance intensity in UV-Vis spectra at 520 nm. In the current paper, colloidal gold nanoparticles were stable for 10 days and their colors were constant, approximately.

Electrode modification

To prepare an Au-PtNPs/NF modified electrode, glassy carbon electrode was polished with emery paper followed by alumina (1.0 and 0.05 μm) and then thoroughly washed with twice-distilled water. Then electrode was placed in ethanol container and used bath ultrasonic cleaner in order to remove adsorbed particles. TMB-based NFs were prepared according to the previous work [28]. Briefly, 2.5 ml of 2 mM aqueous H_2PtCl_6 solution was added into 4 mL of 1.25 mM ethanol TMB solution at room temperature. Several minutes later, doped nanofibers (NFs) were formed with a large amount of blue-violet precipitate. Then, the precipitate was collected by centrifugation, washed several times with water, and dried at 60°C. The suspension of

TMB-based NFs (0.75 mg·ml^{-1}) was prepared by dispersing the resulting powdered NFs into the ethanol solution under ultrasonication for 2 h. Subsequently, 10 µl of the NF dispersion was dropped onto the surface of the GCE and was kept at room temperature until dried (labeled as NFs/GCE). Further modification of AuNPs onto NFs/ GCE was conducted by cyclic volammetry (CV) scanning from 0.2 to -1.0 V at a scan rate of 50 mV·s^{-1} for 16 cycles in 0.1 M KCl solution containing 0.125 mM $HAuCl_4$. During the electrodeposition process, a part of doped Pt (II) ions were simultaneously reduced to Pt atoms, thus leading to a bimetallic Au-PtNP/NF inorganic-organic hybrid nano-composite [23]. After that, the electrode (denoted as Au-PtNPs/ NFs/GCE) was thoroughly rinsed with water and kept at room temperature for further use. For comparison, the modification of AuNPs was also carried out by immersion of NFs/GCE into a suspension of colloidal gold NPs to obtain AuNPs/NFs/GCE, where the doped Pt (II) ions were unchanged. To further modification, Au-PtNPs/NFs/GCE was placed in 0.1 M NaOH containing 10 mM 2,6-diaminopyridine and 4 mM Ni(II)–ammonia complex and the electrode potential was cycled between 0.1 and 0.9 V at a scan rate of 50 mV·s^{-1} for 50 cycles as demonstrated in Scheme 1. After the modification procedure, the electrode (denoted as Ni-DAP/Au-PtNPs/NFs/GCE) was thoroughly rinsed and cycled between 0.1 and 0.9 V in 0.1 M NaOH until a reproducible cyclic voltammogram was obtained.

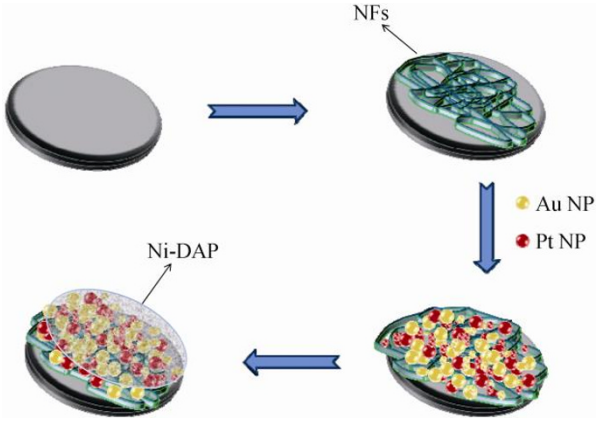

Scheme 1. The overall preparative process of the Ni-DAP/Au-Pt NPs/NFs/GC electrode.

Results and discussion

Characterization of the modified electrode by SEM

To investigate the surface structure and the morphology of the modified electrode, we performed SEM. Figure 1 shows the SEM images of as-prepared NFs (A), Au-PtNP/NF/GCE (B) and Ni-DAP/Au-PtNPs/NFs/GC electrode (C). It can be seen that the as-prepared NFs have diameters of ~150 nm and lengths up to several micrometers. Results show that these nanofibers interlaced together. After the subsequent deposition process, one can see that uniform Au-PtNPs aligned along the surface of those NFs. The generated NPs were homogenously distributed in the matrix of interlaced NFs, constructing a 3D interlaced network (Fig.1B). Figure 1C shows the SEM image of Ni-DAP/Au-PtNPs/NFs/GC electrode. As can be seen, the film has a globular structure with relatively homogeneous distribution. The presence of small nanoparticles leads to an increase in the surface coverage for more adsorption of hydrazine and OH_{ads}. This observed structure indicates that the hydrazine can penetrate through the deposit and access the underlying layer and it can be fully utilized. Therefore, this surface morphology and porosity of modified electrode can result in an improved response for electrooxidation of hydrazine.

Properties of the nano-structured Ni-DAP/Au-PtNPs/NFs/ GC electrode

The Ni-DAP/Au-PtNPs/NFs/GC electrode was prepared as described in experimental part. Consecutive cyclic voltammo-grams using the Au-PtNPs/NFs/GC electrode in 0.1 M NaOH solution containing 10 mM 2,6-diaminopyridine and 4 mM Ni(II)-ammonia complex showed a couple of anodic and cathodic peaks corresponding to the Ni(II)/Ni(III) redox. Film growth is accompanied with increasing current of both peaks, indicating a progressive deposition of the electroactive material, which forms a film as a result of the electrodeposition of the DAP complex. By increasing the number of scans, the anodic and cathodic peaks turned to be more positive and more negative potentials respectively, which may be due to increase in the electrical resistance of the polymer film [29]. Thus, to overcome the resistance, more overpotential is needed. The anodic and cathodic peaks current did not alter upon further potential cycling (more than 50 cycles). The effect of pH on the electrochemical behavior of the Ni-DAP/Au-PtNPs/NFs/GC electrode was investigated. The CVs of the modified GCE were examined at pH ranging from 9 to 13. With the increase of pH values, the anodic and cathodic peak currents increased. Both reduction and oxidation peak potentials of modified electrode became to lower (less positive) potentials and the anodic and cathodic peaks separation decreased. These results indicate that hydroxyl ion plays an important role and thus, in this compound, nickel oxyhydride species act as redox mediator in electrooxidation processes. The same results have been reported for many electrooxidation processes [30, 31]. The redox process of the modified electrode was expressed as follows,

$$Ni(II)(OH)DAP+2OH^- \rightarrow Ni(III)(O)(OH)DAP+H_2O+e^- \quad (1)$$

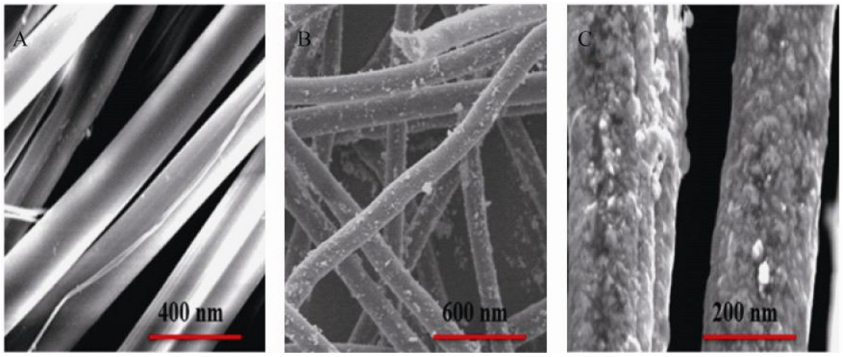

FIG. 1. Typical SEM images: (A) the as-synthesized TMB-based NFs; (B) Au-PtNP/NF inorganic-organic hybrid nanocomposite onto GCE; (C) Ni-DAP/Au-PtNPs/NFs inorganic-organic hybrid nanocomposite onto GCE.

Moreover, the voltammetric behavior of Ni-DAP/Au-PtNPs/NFs/ GC electrode was examined and the result was compared with those of Ni-DAP/AuNP/NF/GC, Ni-DAP/ AuNP-GC and AuNP/GC electrodes. Figure 2 shows cyclic voltammograms of modified electrodes in 0.1 M NaOH solution at a scan rate of 50 mV·s^{-1}. As shown in Fig. 2 at AuNP/GCE, there is no electrochemical response observed (curve a). A pair of well-defined redox peaks with peaks potential separation (ΔE_p) of 91 mV was observed when Ni-DAP/Au-PtNPs/NFs/GC electrode was used (curve d). The observed anodic and cathodic peaks are due to redox reaction of the Ni(III)/Ni(II) couple at the electrode surface. For comparison, Ni-DAP/AuNP/NF/GCE was also fabricated by directly immersing the NFs/CNT-GCE into the colloidal gold suspension for ~10 min. Then the Ni-DAP complex was electrodeposited on the AuNP/NF/GC electrode. Compared with the Ni-DAP/Au-PtNPs/NFs/GC, at the surface of Ni-DAP/AuNP/NF/GCE, not only the peaks potential separation increased (ΔE_p = 140 mV), but also the sensor response decreased about 2 times (curve c). This observation

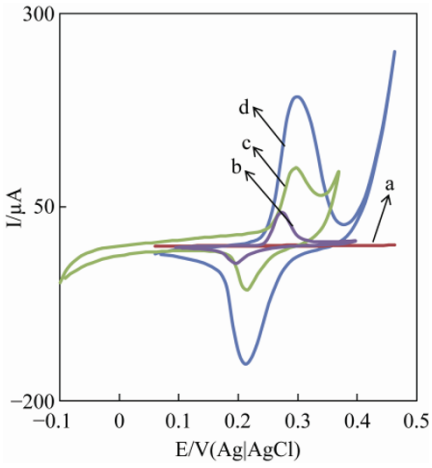

FIG. 2. Cyclic voltammograms of Ni-DAP/Au-PtNPs/NFs/GC (curve d), Ni-DAP/AuNP/NF/GC electrode (curve c), Ni-DAP /AuNP/GC (curve b) and AuNP-GC (curve a) in 0.1 M NaOH solution at a scan rate of 50 mV·s^{-1}.

indicates that the electrode/solution interface became accessible to electrochemical probes with the modification of PtNPs. This fact was confirmed with the SEM results. According to the Randles-Sevcik equation [32], the surface area of the Ni-DAP/Au-PtNPs/NFs/GC electrode was calculated to be 0.0895 cm^2, 3.1 times larger than that of Au-PtNPs/NFs/GCE (0.0286 cm^2). Furthermore, the surface area of Au-PtNPs/ NFs/GCE was 2.2 times larger than NF/GC electrode (0.0125 cm^2). The generated Au-PtNPs were homogenously distributed along the interlaced NFs, constructing individual elements of the electrode. Owing to the smaller spacing between each individual "microelectrode" compared with the size of the NPs, the construction of electrode interface with micro/nanoscale chemical architectures could result in the overlapping diffusion zones and resultant planar diffusion to the array [25]. Similar behavior with lower sensitivity was observed when hydrazine was oxidized at the surface of Ni-DAP/ AuNP-GE electrode (curve b). As it is seen from Fig. 2, the anodic and cathodic peaks potential of Ni(III)/Ni(II) couple at Ni-DAP/Au-PtNPs/NFs/GC and Ni-DAP/AuNP/NF/GC elec-trodes transformed toward positive values relative to those obtained by Ni-DAP/AuNP-GC electrode, which may be due to the increase of path length of electron transfer between redox center and the surface of the bare electrode.

Electrocatalytic oxidation of hydrazine at Ni-DAP/Au-PtNPs/ NFs/GC electrode

Hydrazine did not undergo oxidation at AuNP/GC electrode in the potential window between -0.5 and 1.0 V in 0.1 M NaOH solution (Fig. 3A). However, Ni-DAP on bimetallic Au-Pt inorganic-organic hybrid nanocomposite had a catalytic effect for the oxidation of hydrazine. The voltammetric behaviors of Ni-DAP on the different modified electrodes in the absence and presence of 8.5 mM hydrazine are shown in Fig.3, respectively. As shown, a pair of redox peaks corresponding to the

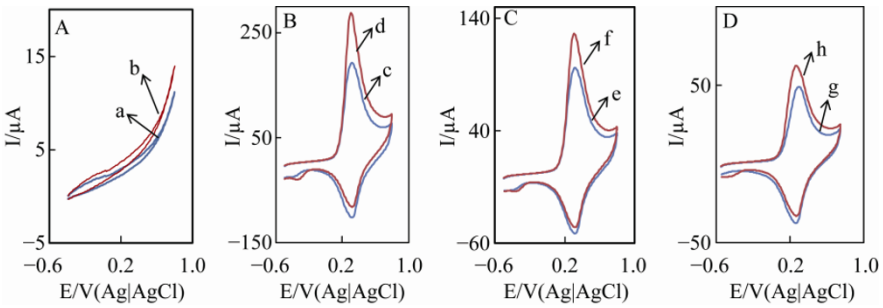

FIG. 3. Cyclic voltammograms of AuNP/GC electrode (A) Ni-DAP/Au-PtNPs/NFs/GC electrode(B), Ni-DAP/AuNP/NF/GC electrode (C) and Ni-DAP/AuNP/GC (D) in the absence (curves a, c, e and g)and presence (curves b, d, f and h) of 8.5 mM hydrazine in 0.1 M NaOH solution at a scan rate of 50 $mV \cdot s^{-1}$.

Ni(III)/Ni(II) couple was observed in the absence of hydrazine (curves a, c, e and g). As it can be seen, upon the addition of hydrazine, an enhancement in the anodic peak current is observed and the cathodic peak current tended to decrease (curves d, f and h). This observation indicates that, along with the anodic potential sweep, hydrazine reduces Ni(III) to Ni(II), while the simultaneous oxidation of the regenerated Ni(II) causes an increase in the anodic current. For the same reason, the cathodic current is smaller in the presence of hydrazine, indicating that Ni(III) is consumed during a chemical step [33]. Moreover, the oxidation peak current of hydrazine at Ni-DAP/Au-PtNPs/NFs/GC electrode was (Fig. 3B), 282 μA, which is 2.2 times larger than that at Ni-DAP/AuNP/NF/GC electrode (Fig. 3C) of 125 μA. As it is seen from Fig. 3, the similar behavior with low sensitivity was observed when hydrazine was oxidized at the surface of Ni-DAP/AuNP-GC electrode (Fig. 3D). The result indicates that the presence of bimetallic Au-Pt inorganic-organic hybrid nanocomposite in the modified electrode supplied a larger surface area to allow more deposition of Ni-DAP complex to oxidizing hydrazine.

In order to optimize the electrocatalytic response of the modified electrode toward the electrocatalytic oxidation of hydrazine, the effect of pH on the peak current and peak potential was investigated. The cyclic voltammograms of the Ni-DAP/Au-PtNPs/NFs/GC in 7 mM hydrazine at different pH values (8-13) were recorded. As can be seen from Fig. 4, the peak current gradually increased with the increase of pH and reached a wide maximum at pH 13.

The peak potential shifted to the less positive value with the increase of pH. Since more reproducible results and high catalytic activity of the modified electrode was observed at pH 13, this pH value was chosen as optimum pH for hydrazine determination. The same results have been reported for hydrazine electrooxidation processes [34, 35].

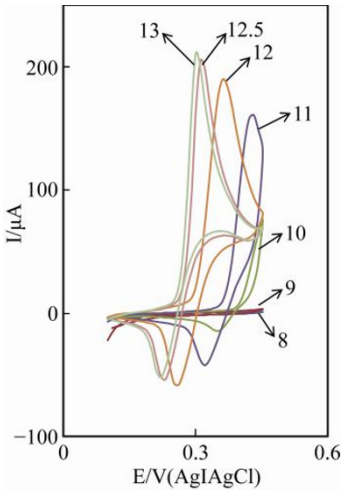

FIG. 4. Cyclic voltammograms of the Ni-DAP/Au-PtNPs/NFs/GC electrode in the presence of 7 mM of hydrazine in various pHs at a scan rate of 50 $mV \cdot s^{-1}$.

Cyclic voltammograms of different concentrations of hydrazine (ranging from 2.1 to 64.7 mM) at the modified electrode in 0.1 M NaOH solution were recorded. The calibration curve based on the anodic peak current was linear with the concentration of hydrazine in the range from 2.1 to 64.7 mM with a correlation coefficient of 0.995. Examination of the resulted cyclic voltammograms showed that hydrazine oxidation onset potentials increased when increasing hydrazine concentration. The onset delay followed from higher Ni-DAP electron transfer resistance as hydrazine absorbs on the Ni(II) active center. By this model, high hydrazine concentrations resulted in great numbers of Ni(II) active centers with absorbed hydrazine, with increasing onset delay following from increasing hydrazine concentration. Also, the current amplitude of the cathodic peak showed significant decrease with the increasing hydrazine concentrations, which indicating that Ni(III) was consumed during a chemical process. The possible mechanism of hydrazine electrooxidation on Ni-DAP/Au-PtNPs/NFs/GC electrode may be as follows,

$$Ni(II)(OH)DAP+2OH^- \rightarrow Ni(III)(O)(OH)DAP+H_2O+2e^- \quad (2)$$

$$2Ni(III)(O)(OH)DAP+N_2H_4\rightarrow N_2+2Ni(II)(OH)DAP+2H_2O \quad (3)$$

Figure 5A illustrates cyclic voltammograms of 6.7 mM hydrazine using modified electrode recorded at potential sweep rates ranging from 5 to 200 $mV{\cdot}s^{-1}$. The oxidation current of hydrazine on the modified surface increases linearly with the square root of the potential sweep rate (Fig. 5B), which indicates the mass transfer controlled process. Also, it can be seen that, with the increasing scan rate, the anodic peak potential tend toward positive potentials, suggesting a kinetic limitation in the reaction between the redox sites of the Ni-DAP/Au-PtNPs/NFs/GC electrode and hydrazine. The α value of the electrodic reaction can be evaluated from the following equation [36],

$$E_p=(b/2)\log(\nu)+\text{constant} \quad (4)$$

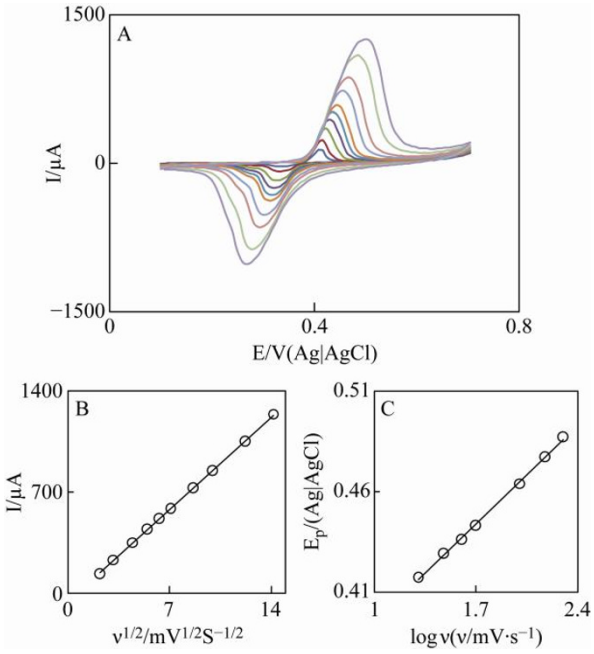

FIG. 5. (A) Cyclic voltammgrams of the modified electrode in the presence of 6.7 mM hydrazine in 0.1 M NaOH solution at various scan rates: (1-10) 5, 10, 20, 30, 40, 50, 75, 100, 150 and 200, respectively. (B) The variation of anodic peak currents vs. square root of potential scan rate (C) the dependence of the anodic peak potential versus log (υ).

where b indicates the tafel slope. Using the dependency of anodic peak potential on the natural logarithm of the potential sweep rate (Fig. 5C), the value of electron transfer coefficient (α) is estimated as 0.47. Also, the obtained value of transfer coefficient from the recorded I-E curve of electrocatalytic oxidation of hydrazine (slope of log I vs. E plot) confirms the above reported value (0.508).

Rotating disk electrode (RDE) voltammetry

The electrocatalytic activity of the Ni-DAP/Au-PtNPs/NFs/GC electrode toward the oxidation of hydrazine was also evaluated using RDE voltammetry technique. The steady state I-E curves were recorded for the oxidation of hydrazine at modified rotating GC disk electrode. Typical examples of the I-E curves (RDE voltammograms) for hydrazine concentration of 9.8 mM at the Ni-DAP/Au-PtNPs/NFs/GC electrode are presented in Fig. 6A. The limiting current obtained on the modified electrode increases with rotation speed of the electrode increased. The linearity of the Levich plots at low rotation rates indicates that the limiting current is mass-transport controlled (Fig. 6B). The Levich plots deviated from linearity at high rotation rates, suggesting a kinetic limitation. Under these conditions the Koutecky–Levich equation [37] can be used to determine the rate constant. The limiting current is given by Eq. (5),

$$1/I_{lim}=1/I_{Lev}+1/I_K \quad (5)$$

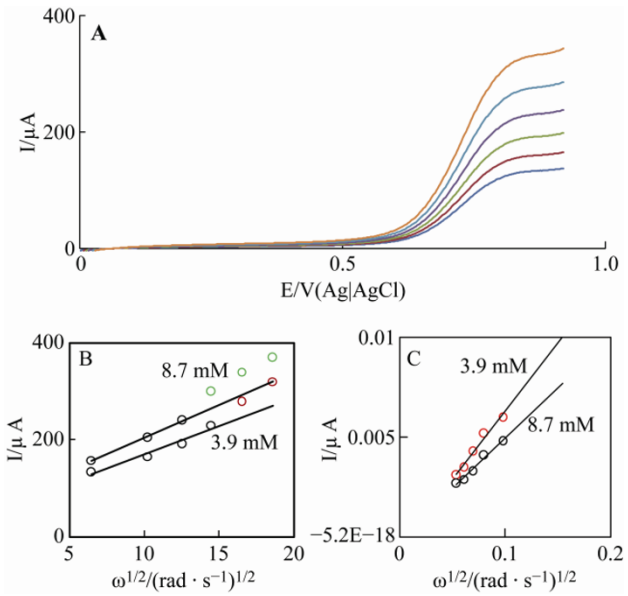

FIG. 6. (A) Rotating disk electrode voltammograms recorded at Ni-DAP/Au-PtNPs/NFs/GC electrode for 9.8 mM hydrazine in 0.1 M NaOH solution at a scan rate of 50 $mV{\cdot}s^{-1}$. The rotation speed is in rpm: (1-6) 200, 400, 600, 800, 1200 and 2000, respectively. (B) and (C): Levich and Koutecky-Levich plots (respectively) for various concentrations of hydrazine.

where I_{Lev} is the Levich current and I_K is the kinetic current. I_{Lev} and I_K are defined by Eqs. (6) and (7),

$$I_{Lev} = 0.62\ nFAD^{2/3}\ \upsilon^{-1/6}\omega^{1/2}c_0 \quad (6)$$

where n is the number of electrons, D is the diffusion coefficient of the substrate (hydrazine), F is the faradaic constant, C_0 is the bulk concentration of the substrate, A is the electrode area, v is the kinematic viscosity of the solution and ω is the rotation rate.

$$I_k = nFAc_0K\Gamma \quad (7)$$

where K is the rate constant ($dm^3 \cdot mol^{-1} \cdot s^{-1}$) governing the reaction of the catalyst with hydrazine, and the quantity of the catalyst on the electrode surface ($mol \cdot cm^{-2}$). In the case of a mass transfer controlled electrochemical reaction, the relationship between the limiting current and rotating speed should obey the Levich equation (Eq. (6)). Based on the Eq. (6), the plot of the limiting current as function of the $\omega^{1/2}$ should be a straight line. This occurred in the case of low rotation speed of electrode and corresponded to the initial part of Levich plots. The diffusion coefficient of hydrazine in the solution can be obtained from the slope of Levich plot. The value of D in this medium was found to be 1.75×10^{-6} $cm^2 \cdot s^{-1}$. According to the Levich plots (Fig. 6B), the current increases when increasing electrode rotation speed, but are found to be non-linear, indicating kinetic limitations. In this case, the catalytic current I_{cat} related to the mediated reaction is a function of both Levich current (I_{Lev}), and kinetic current (I_K). Therefore mass transfer of hydrazine in the solution and the electron cross-exchange between hydrazine and the Ni-DAP redox sites become dominant, and the Koutecky-Levich equation may be used. According to Eq. (5), the plot of I_l^{-1} versus $\omega^{-1/2}$ gives a straight line (Fig. 6C). The value of the rate constant for the catalytic reaction, k can be obtained from the intercept of the Koutecky-Levich plot. The value of k was found to be in the range 6.51×10^2 to $3.86\times10^2 M^{-1} \cdot s^{-1}$ for hydrazine concentration in the range of 3.9-8.7 mM. Diffusion coefficient of hydrazine, D, may be obtained from the slope of Koutecky-Levich plots. The mean value of D was found to be 4.51×10^{-6} $cm^2 \cdot s^{-1}$, which is in agreement with that obtained from Levich plot. An average value for D was calculated equal to 3.13×10^{-6} $cm^2 \cdot s^{-1}$.

Amperometric detection of hydrazine at modified electrode

Since amperometry under stirred conditions has a higher current sensitivity than cyclic voltammetry, it was used to estimate the low limit of detection. Figure 7A displays a typical steady-state catalytic current time response of the rotated modified electrode (2000 rpm) with successive injection of hydrazine, at an applied potential of 0.35 V vs. reference electrode. (The initial potential for hydrazine oxidation at this modified GCE was about 0.2 V vs. reference electrode. At this potential, hydrazine was not yet electroactive. By setting the working electrode potential at 0.25 V, hydrazine was reduced, but not so effective that its surface concentration was zero; thus, the peak potential (0.35 V) was chosen to be at a constant value where the surface concentration was zero. Hence, hydrazine arrived as fast as diffusion could bring it, and the current was limited by this factor [32].) As shown, during the successive addition of hydrazine, a well-defined response was observed, demonstrating stable and efficient catalytic ability of the electrocatalyst immobilized on the bimetallic Au-Pt inorganic-organic hybrid nanocomposite film. The response current is linear in the range of 0.2-85 μM of hydrazine (Fig. 7B). The

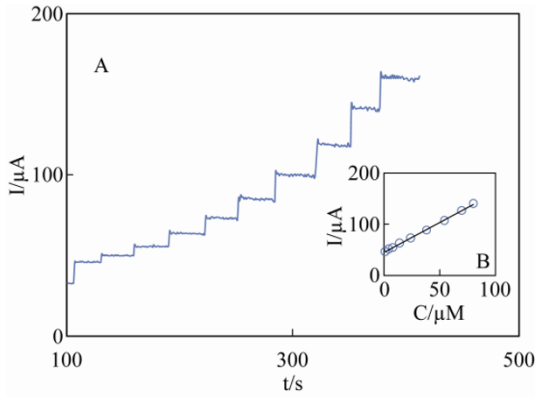

FIG. 7. (A) Amperometric response at rotating modified electrode in the presence of different hydrazine concentration: 0.2, 5, 10, 15, 22, 30, 43, 68 and 85 μM, respectively. Conditions: 0.35 V constant potential, pH 13 and rotation speed is 2000 rpm, (B) plots of current vs. hydrazine concentration.

calibration plot over the concentration range of 0.2-85 μM has a slope of correlation coefficient of 0.998 and the detection limit of 0.1 μM at signal to noise ratio of 3. Detection limit and linear calibration range of the proposed method were compared with those that obtained in other reports, and the results are summarized in Table 1. As seen, the analytical parameters are comparable or better than results reported for hydrazine determination at the surface recently fabricated modified electrodes [38-46].

Interference effect for hydrazine determination

To apply this modified electrode to determine hydrazine in environmental water samples, the influence of common ions for the determination of 7×10^{-6} M hydrazine was investigated. If these interfering ions cause a relative error of less than 5% for the determination of 7×10^{-6} M of hydrazine, the interference of these species are negligible. The results are summarized in Table

2. It is shown that most of the investigated ions did not interfere for determination of hydrazine.

Table 1 Comparison of the responses of some hydrazine sensors constructed based on different modified electrode materials.

Electrode material	Detection limit (μM)	Linear range (μM)	Ref.
ZnO nanonails	0.2	0.1-1.2	[38]
High-aspect-ratio ZnO	0.0847	0.5-1.2	[39]
Hematoxylin multi-wall carbon nanotubes	0.68	2.0-122.8	[40]
Au/PPy/GCE	0.2	1-500	[41]
Copper oxide nanoarray	0.17	---	[42]
BiHCF-modified CCEs	3	---	[43]
Ru-complex films	8.5	10-10,000	[44]
Nickel hexacyanoferrate	2.28	2-5000	[45]
carbon nanotube-wired ZnO nanoflower	0.18	0.6-250	[46]
This work	0.1	0.2-85	

Table 2 The extent of interfering substance concentration in the determination of hydrazine

Matrix compounds	Ratio[a] (10^3)
Na^+, K^+, Mg^{2+},	10
Ca^{2+}, Br^+,	9
Hg^+, Cd^{2+}, Mn^{2+}	5
I^-, $SO4^{2-}$	1
Fe^{3+}, CO^{2-},	0.5

[a]Ratio denotes the ratio of the concentration between the interfering substance and hydrazine, i.e., [ion]/[N_2H_4].

Analytical applications

Since the present amperometric method is very sensitive and a small volume of the sample is adequate for the hydrazine determination, the standard addition method is suitable for simple and rapid evaluation of hydrazine. The reliability of the amperometric determination of hydrazine in photographic developer was verified using an iodimetric procedure described in the literature [47]. For this purpose, a 0.05 M iodine solution which was standardized in the usual way with a primary standard of As_2O_3 or titrisol thiosulfate solution was used. The result of statistical calculation shown in Table 3 indicates good precision and good agreement between the repeatability of the proposed and official methods.

Stability and reproducibility

The stability and the reproducibility of the Ni-DAP/Au-PtNPs/NFs/ GCE were studied in 0.1 M NaOH solution .The results indicated that after 80 continuous cycles at 50 $mV \cdot s^{-1}$, the peak heights of the Ni-DAP/Au-PtNPs/NFs/GCE decreased less than 5%. In addition, a set of 15 replicate amperometric measurements for 5 μM hydrazine yielded a relative standard deviation (R.S.D.) of 2.9%. Thus, the Ni-DAP/Au-PtNPs/NFs/GCE exhibited acceptable stability and reproducibility for hydrazine detection.

Table 3 Determination of hydrazine in photographic developer

Number	Found[a]/M	RSD(%)	Found[b]/M	RSD(%)
1	0.025		0.022	
2	0.019		0.023	
3	0.024		0.021	
4	0.023	9.8	0.024	5.65
5	0.021		0.0205	
6	0.02		0.021	
average	0.022		0.0219	

[a]By amperometric method; [b]By iodimetric titration method.

Conclusions

A new composite material modified electrode as Ni-DAP/Au-PtNPs/NFs/GCE was prepared by electrodepositing of Ni-DAP complex on the surface of bimetallic Au-Pt inorganic-organic nanofiber hybrid nanocomposite glassy carbon electrode in alkaline solution. Compared with Ni-DAP/AuNP-GCE and Ni-DAP/AuNP/NF/GCE, the properties of bimetallic Au-Pt inorganic-organic nanofiber resulted in improvement of both the reversibility and current responses of Ni-DAP/Au-PtNPs/NFs/GC electrode. The Ni-DAP/Au-PtNPs/NFs/GC electrode also enhanced electrocatalytic activity toward the oxidation of hydrazine. Some kinetic parameters such as the electron transfer coefficient, the diffusion coefficient of hydrazine and the catalytic rate, constant k_{cat} of the catalytic reaction were calculated. A sensitive amperometric method was proposed for the determination of hydrazine with the advantages of fast response and excellent reproducibility.

The authors gratefully acknowledge the support of this work by the Islamic Azad University, Khorramabad Branch research for financial support.

Received 30 November 2010; accepted 8 January 2011; published online 20 January 2011.

References

1. A. Safavi and, A. A.Ensafi, Anal. Chim. Acta 300, 307 (1995).

2. W. X. Yin, Z. P. Li, J. K. Zhu and H. Y. Qin, J. Power Sources 182, 520 (2008). doi:10.1016/j.jpowsour.2008.04.028
3. J. S. Budkuley, Microchim, Acta 108 103 (1992). doi:10.1007/BF01240376
4. J. W. Mo, B. Ogorevc, X. Zhang and B. Pihlar, Electroanalysis 12, 48 (2000). doi:10.1002/(SICI)1521-4109(20000101)12:1<48::AID-ELAN48>3.0.CO;2-H
5. A. L. Ensafi and B. Rezaei, Talanta 47, 645 (1998). doi:10.1016/S0039-9140(98)00113-1
6. A. Safavi and M. A. Karimi, Talanta 58, 785 (2002). doi:10.1016/S0039-9140(02)00362-4
7. M. H. Pournaghi-Azar and R. Sabzi, J. Electroanal. Chem. 543, 115 (2003). doi:10.1016/S0022-0728(02)01480-8
8. S. J. R. Prabakar and S. S. Narayanan, J. Electroanal. Chem. 617, 111 (2008). doi:10.1016/j.jelechem.2008.01.020
9. N. Maleki, A. Safavi, E. Farjami and F. Tajabadi, Anal. Chim. Acta 611, 151 (2008). doi:10.1016/j.aca.2008.01.075
10. M. Revenga-Parra, T. Garcia, E. Lorenzo and F. Pariente, Sens. Actuators B 130, 730 (2008). doi:10.1016/j.snb.2007.10.038
11. M. Y. Elahi, H. Heli, S. Z. Bathaie and M. F. Mousavi, J. Solid State Electrochem. 11, 273 (2007). doi:10.1007/s10008-006-0104-4
12. A. L. Briseno, S. C. B. Mannsfeld, E. Formo, Y. J. Xiong, X. M. Lu, Z. N. Bao, S. A. Jenekhe and Y. N. J. Xia, Mater. Chem. 18, 5395 (2008). doi:10.1039/b809228c
13. T. Yoshida, J. Zhang, D. Komatsu, S. Sawatani, H. Minoura, T. Pauporte, D. Lincot, T. Oekermann, D. Schlettwein, H. Tada, D. Wohrle, K. Funabiki, M. Matsui, H. Miura and H. Yanagi, Adv. Funct. Mater. 19, 17 (2009). doi:10.1002/adfm.200700188
14. D. J. Milliron, I. Gur and A. P. Alivisatos, MRS Bull. 30, 41 (2005).
15. A. L. Briseno, S. C. B. Mannsfeld, X. Liu, Y. Xiong, S. A. Jenekhe, Z. Bao and Y. Xia, Nano Lett. 7, 668 (2007). doi:10.1021/nl0627036
16. G. Lu, C. Li, J. Shen, Z. Chen and G. Shi, J. Phys. Chem. C 111, 5926 (2007). doi:10.1021/jp070387t
17. R. J. Tseng, J. Huang, J. Ouyang, R. B. Kaner and Y. Yang, Nano Lett. 5, 1077 (2005). doi:10.1021/nl0505871
18. J. Polleux, A. Gurlo, N. Barsan, U. Weimar, M. Antonietti and M. Niederberger, Angew. Chem. Int. Ed. 45, 261 (2006). doi:10.1002/anie.200502823
19. S. Forster and M. Antonietti, Adv. Mater. 10, 195 (1998). doi:10.1002/(SICI)1521-4095(199802)10:3<195::AID-ADMA195>3.0.CO;2-V
20. C. Sanchez, B. Juli´an, P. Belleville and M. Popall, J. Mater. Chem. 15, 3559 (2005). doi:10.1039/b509097k
21. J. W. Kriesel and T. D. Tilley, Adv. Mater. 15, 1645 (2003).
22. P. Gomez-Romero, Adv. Mater. 15, 163 (2003).
23. J. Gong, T. Zhou, D. Song, L. Zhang and X. Hu, Anal. Chem. 82, 567 (2010) doi:10.1021/ac901846a
24. H. Sabahudin, L. Yali, B. M. Keith and H. T. L. John, Anal. Chem. 76, 1083 (2004). doi:10.1021/ac035143t
25. X. Dai, G. G. Wildgoose, C. Salter, A. Crossley and R. G. Compton, Anal. Chem. 78, 6102 (2006). doi:10.1021/ac060582o
26. V. R. Holland, B. C. Saunders, F. L. Rose and A. L. Walpole, Tetrahedron 30, 3299 (1974). doi:10.1016/S0040-4020(01)97504-0
27. E. Majid, S. Harpovic, Y. Liu, K. B. Male and J. H. T. Luong, Anal. Chem. 78, 762 (2006). doi:10.1021/ac0513562
28. J. H. Yang, H. S. Wang, L. H. Lu, Y. B. Wang, W. D. Shi and H. J. Zhang, Synth Met. 158, 572 (2008). doi:10.1016/j.synthmet.2008.04.005
29. T. F. Otero and E. D. Larreta-Azelain, Polymer 29, 1522 (1988). doi:10.1016/0032-3861(88)90320-5
30. S. Majdi, A. J. Abbari, H. Heli and A. A. Moosavi-Movahedi, Electrochim. Acta. 52, 4622 (2007). doi:10.1016/j.electacta.2007.01.022
31. J. B. He, X. Q. Lin and J. Pan, Electroanalysis 17, 1681 (2005). doi:10.1002/elan.200503274
32. A. J. Bard, L. R. Faulkner, "Electrochemical Methods-Fundamentals and Applications", John Wiley and Sons, New York (2000).
33. T. R. I. Cataldi, D. Centonze and G. Ricciardi, Electro-analysis, 7, 312 (1995). doi:10.1002/elan. 1140070403
34. V. Rosca, M. T. M. Koper, Electrochim. Acta 53, 5199 (2008). doi:10.1016/j.electacta.2008.02.054
35. Y. Wanga, Y. Wan and D. Zhang, Electrochem. Commun.12, 187 (2010). doi:10.1016/j.elecom.2009.11.019
36. J. A. Harrison and Z. A. Khan, J. Electroanal. Chem. 28, 131(1970). doi:10.1016/S0022-0728(70)80288-1
37. A. J. Bard and L. R. Faulkner, "Electrochemical methods, in: Fundamentals and Applications", Wiley, New York (1980).

38. A. Umar, M. M. Rahman, S. H. Kim and Y. B. Hahn, Chem. Commun. 2, 166 (2008). doi:10.1039/b711215g
39. A. Umar, M. M. Rahman and Y. B. Hahn, Talanta, 77, 1444 (2009).
40. H. Zare and N. Nasirrizadeh, Electrochim. Acta 52, 4153 (2007). doi:10.1016/j.electacta.2006.11.037
41. J. Li and X.Q. Lin, Sens. Actuators B, 126, 527 (2007). doi:10.1016/j.snb.2007.03.044
42. G. F. Wang, A. X. Gu, W. Wang, Y. Wei, J. J. Wu, G. Z. Wang, X. J. Zhang and B. Fang, Electrochem. Commun. 11, 631 (2009). doi:10.1016/j.elecom.2008.12.061
43. J. B. Zheng, Q. L. Sheng, L. Li and Y. Shen, J. Electroanal. Chem. 611, 155 (2007). doi:10.1016/j.jelechem.2007.08.013
44. J. S. Pinter, K. L. Brown, P. A. D. Young and G. F. Peaslee, Talanta, 71, 1219 (2007). doi:10.1016/j.talanta.2006.06.017
45. A. Salimi and K. Abdi Talanta 63, 475 (2004). doi:10.1016/j.talanta.2003.11.021
46. B. Fang, C. Zhang, W. Zhang and G. Wang, Electrochimica. Acta 55, 178 (2009). doi:10.1016/j.electacta.2009.08.036
47. F. J. Welcher, Standard Methods of Chemical Analysis, 6th ed., New York, 493 (1963).